AGU PUBLICATIONS

JGR

Journal of Geophysical Research: Biogeosciences

RESEARCH ARTICLE
10.1002/2017JG003834

Key Points:
- Aerosol deposition over the past 35 years reveals an increasing trend in the mean intensity of these events over Alboran Sea
- Nearshore autotrophic picoplankton is more sensitive to UVR impact than those from offshore
- UVR × dust exerted a positive effect on autotrophic picoplankton in nearshore but negative in offshore

Supporting Information:
- Supporting Information S1

Correspondence to:
P. Carrillo,
pcl@ugr.es

Citation:
González-Olalla, J. M., J. M. Medina-Sánchez, M. J. Cabrerizo, M. Villar-Argáiz, P. M. Sánchez-Castillo, and P. Carrillo (2017), Contrasting effect of Saharan dust and UVR on autotrophic picoplankton in nearshore versus offshore waters of Mediterranean Sea, *J. Geophys. Res. Biogeosci.*, *122*, doi:10.1002/2017JG003834.

Received 4 MAR 2017
Accepted 25 JUL 2017
Accepted article online 31 JUL 2017

Contrasting effect of Saharan dust and UVR on autotrophic picoplankton in nearshore versus offshore waters of Mediterranean Sea

J. M. González-Olalla[1], J. M. Medina-Sánchez[2], M. J. Cabrerizo[1,2], Manuel Villar-Argáiz[2], Pedro M. Sánchez-Castillo[3], and Presentación Carrillo[1]

[1]Universitary Institute of Water Research, University of Granada, Granada, Spain, [2]Department of Ecology, University of Granada, Granada, Spain, [3]Department of Botanic, University of Granada, Granada, Spain

Abstract Autotrophic picoplankton (APP) is responsible for the vast majority of primary production in oligotrophic marine areas, such as the Alboran Sea. The increase in atmospheric dust deposition (e.g., from Sahara Desert) associated with global warming, together with the high UV radiation (UVR) on these ecosystems, may generate effects on APP hitherto unknown. We performed an observational study across the Alboran Sea to establish which factors control the abundance and distribution of APP, and we made a microcosm experiment in two distinct areas, nearshore and offshore, to predict the joint UVR × dust impact on APP at midterm scales. Our observational study showed that temperature (*T*) was the main factor explaining the APP distribution whereas total dissolved nitrogen positively correlated with APP abundance. Our experimental study revealed that Saharan dust inputs reduced or inverted the UVR damage on the photosynthetic quantum yield (Φ_{PSII}) and picoplanktonic primary production (PP_P) in the nearshore area but accentuated it in the offshore. This contrasting effect is partially explained by the nonphotochemical quenching, acting as a photorepair mechanism. Picoeukaryotes reflected the observed effects on the physiological and metabolic variables, and *Synechococcus* was the only picoprokaryotic group that showed a positive response under UVR × dust conditions. Our study highlights a dual sensitivity of nearshore versus offshore picoplankton to dust inputs and UVR fluxes, just at the time in which these two global-change factors show their highest intensities and may recreate a potential future response of the microbial food web under global-change conditions.

1. Introduction

Alboran Sea (south-western Mediterranean region) displays two quasi-permanent anticyclonic gyres determined mainly by the Atlantic current, topography, the Earth's rotational effect, and the predominant west winds [*García-Górriz and Carr*, 2001]. Traditionally, these subtropical gyres are considered oligotrophic areas where autotrophic picoplankton (APP) (*Prochlorococcus*, *Synechococcus*, and picoeukaryotes) accounts for the major part of the phytoplankton biomass and primary production (PP) [*Agawin et al*., 2000; *Alvain et al*., 2005; *Grossman et al*., 2010; *Buitenhuis et al*., 2013]. The small size and higher surface:volume ratio of APP give them a competitive advantage against nanoplankton growing at low nutrient concentrations [*Agustí and Llabrés*, 2007]. Also, due to their smaller size, APP inhabiting low-resource environments are more efficient than larger-sized cells in photon absorption because of reduced chromophore self-shading [*Raven*, 1998]. Nevertheless, its size may also pose a disadvantage under high levels of photosynthetically active radiation (PAR) or ultraviolet radiation (UVR), as APP possesses a low capacity for screening out damaging radiation probably due to a lower ability to distribute the intracellular UVR absorbed [*Wu et al*., 2016] and its inefficient photorepair mechanisms [*Raven*, 1998].

The Mediterranean region is an area particularly sensitive to global change [e.g., *Belkin*, 2009]. In fact, the increase in severe droughts and positive anomalies in the North Atlantic Oscillation index [*Mukhopadhyay and Kreycik*, 2008], together with its position on the boundary between two climatic regimes [*Giorgi and Lionello*, 2008] and bordering the largest desert area in the world, leads to frequent inputs of mineral-dust particles, prevalently during the summer [*Bullejos et al*., 2010; *Gallisai et al*., 2014]. Recent evidence from dust-addition experiments [*Lekunberri et al*., 2010; *Marañón et al*., 2010] have indicated that dust inputs provide multiple nutrients to marine ecosystems [*Mackey et al*., 2015]. Of special interest are the dust-derived phosphorus (P) effects on P-limited oligotrophic ecosystems, such as the Mediterranean Sea [*Tanhua et al*.,

2013]. Hence, dust deposition may alter phytoplankton physiology (e.g., Photosystem II functioning (Φ_{PSII}) [*Strzepek and Harrison*, 2004; *Behrenfeld et al*., 2009]), community structure [*Finkel et al*., 2010], marine productivity, and carbon sequestration [*Jickells et al*., 2005; *Jickells and Moore*, 2015; *Cabrerizo et al*., 2016]. Although dust deposition increases macronutrients [e.g., P; *Prospero and Lamb*, 2003] as well as micronutrients (e.g., iron and calcium [*Pulido-Villena et al*., 2006; *Shao et al*., 2011]), and thus improves phytoplankton growth, it is not clear whether the excessive concentration of trace metals (e.g., copper) and contaminants contained in dust may also harm the metabolism and physiology of marine planktonic communities [*Paytan et al*., 2009], counterbalancing the positive effect of nutrients.

In the current global-change scenario, higher dust inputs together with many other anthropogenic stressors can simultaneously interact. In fact, global warming is expected to increase UVR exposure as result of a shallower upper mixed layer (UML) due to greater stratification of the water column [*Barbieri et al*., 2002; *Häder et al*., 2011; *Carrillo et al*., 2015a]. In addition, the oligotrophic nature of waters and the high-incident fluxes of UVR in the Mediterranean region favor the deep penetration of radiation into the water column [*Tedetti and Sempéré*, 2006; *Carrillo et al*., 2015b]. The contribution of UV-B (280–315 nm) and, to a lesser extent, UV-A (315–400 nm) to photoinhibition on primary producers is notable in the uppermost layer [*Figueroa et al*., 1997a, 1997b; *Gang et al*., 2011]. Previous studies have shown that UVR has a negative impact on several targets and processes (e.g., DNA synthesis, photosynthesis, and nutrient uptake) [*Hessen et al*., 1997; *Buma et al*., 2001; *Day and Neale*, 2002], including biomass, species composition, and growth rates of phytoplankton [*Buma et al*., 2003; *Leu et al*., 2007]. However, beneficial UVR effects have also been reported (e.g., increased DNA photorepair [*Helbling and Zagarese*, 2003]). Therefore, the interaction between high UVR and increased dust aerosol deposition could create a new balance between damage and repair on the phytoplankton community, which is unknown.

Due to global warming, a greater extension of the subtropical oligotrophic gyres is expected to lead to a more important role of APP in global biogeochemical cycles [*Morán et al*., 2010]. In this context, we analyze the distribution pattern of APP in Alboran Sea region and its relation with the main abiotic factors of global change with the aim of experimentally determining the nature and direction of interactive effects of Saharan dust and UVR on APP communities of nearshore (outside of the Western Anticyclonic Gyre) and offshore (inside the Western Anticyclonic Gyre) areas at short-term (hours) and midterm (days) scales. These areas were chosen for the potential differences in trophic and optical characteristics between them determined by the geostrophic currents in the region. The Western Anticyclonic Gyre may provide cold nutrient-rich water near the southern coast of Spain [*Sarhan et al*., 2000; *García-Górriz and Carr*, 2001], exerting a greater fertilizing effect on the photic layer and stimulating primary productivity [*Packard et al*., 1988], compared to offshore area. However, the existence, intensity, and shape of this gyre and the supply of nutrients are also controlled by horizontal circulation and seasonal stratification [*García-Górriz and Carr*, 2001]. These mass-water dynamics may bring about two areas with different optical characteristics, with the area of the nearshore usually presenting greater opacity, due to, among other things, the runoff water and wave action [*Romero et al*., 2011], which in turn determine lesser exposure of phytoplankton to harmful levels of UVR than in Open Sea habitats [*Erga et al*., 2005; *Tedetti and Sempéré*, 2006]. Thus, phytoplankton from the coastal area could be more sensitive to UVR under a shallower UML [*Häder et al*., 2014]. Therefore, our working hypothesis is that APP community will be more UVR-damaged in the nearshore area than in the offshore area, because the cells in the latter area would be adapted to high UVR. The dust inputs, mainly through the macronutrient supply, will attenuate the harmful UVR effect, and the magnitude of this effect will be greater in the nearshore areas than in the offshore. To test this hypothesis, we performed an experiment lasting 5 days, evaluating the short-term (24 h) and midterm responses (5 days) of APP to manipulation of the radiation quality and dust supply. In this way, we evaluated the individual and interactive effects of both factors on the Φ_{PSII} yield, nonphotochemical quenching (NPQ), picoplanktonic primary production (PP_P), and changes in the taxonomical composition of APP communities.

2. Materials and Methods

2.1. Study Area for Observational and Experimental Study

The observational and experimental studies were conducted aboard the B/O Francisco de Paula Navarro (Spanish Institute of Oceanography) during the MICROSENS survey (17–21 June 2014). The cruise sailed

from Malaga on 17 June and arrived at Almeria on 21 June. A total of 14 stations distributed along the Alboran Sea were sampled. For the observational study, seawater samples from each station were collected using 10 L-Niskin bottles, at depths of 3 and 15 m, because the UML depth in Alboran Sea tends to oscillate between 14 (±5) and 30 (±15) m [*Báez et al*., 2013; *Houpert et al*., 2015] during the same stage as our sampling period. Samples from each station were used for the observational study (see details below).

Our experimental study was conducted with samples taken from stations 1 (nearshore, 36°37′N, 4°24′W) and 3 (offshore, 35°59′N, 4°19′W), starting the experiment on 17 June and carrying out biological, chemical, and physical measurements every day until 21 June. The seawater samples (from surface to 15 m depth) were filtered through a 200 μm pore size mesh to remove mesozooplankton and mixed in two acid-cleaned 150 L-PVC tanks. Zooplankton was removed to improve the replicability of the microcosm since its presence can generate unequal effects on the phytoplankton community. Then, prefiltered 15 L seawater from each area was dispensed into 20 L low-density polyethylene (LPDE) (Plasticos Andalucía, Spain) microcosms which were placed floating inside two black-walled tanks with running water to maintain the in situ temperature. LPDE transmits ~90% of PAR, 75% of UV-A, and 60% of UV-B. Microcosms were manually shaken every hour to prevent organisms from settling so that they would receive homogeneous irradiance. The samples were taken using a syringe connected to an acid-washed silicone tube inserted in each microcosm to avoid their being tampered with.

For an assessment of the combined impact of UVR and Saharan dust in each area, a 2 × 2 full factorial experimental design was implemented with (a) two light treatments, +UVR (>280 nm) versus −UVR (>400 nm) and (b) two dust treatments (dust and no-dust additions). Each treatment was applied in triplicate. For the -UVR treatment, the tank was covered with a sheet of Ultraphan Opak Difegra 395 filter, which screens out UVR < 390 nm and transmits ~90% of the PAR. For the +UVR treatments, the tank was covered with LDPE (Plásticos Andalucía, Spain) to ensure that the intensity of PAR received was identical in both tanks. Also, half of microcosms for each area were amended with 4.1 mg L^{-1} (61.5 g m^{-2}) of Saharan dust collected in situ from soil in the Moroccan region of Merzouga (Tafilalet, Morocco; 31°06′00″N, 3°59′24″W). The dust added was obtained from soil fractioning by means of a similar procedure as in *Guieu et al*. [2010]), in order to reproduce fine, long-range transported desert dust particles. Thus, the soil was sieved with a nested column with wire mesh cloth of 100 mm and 1 mm pore size, and dust was collected on a pan underneath the nest of sieves. The particles collected were then winnowed next to a tilted glass, and the particles that adhered to the glass were gently collected with a fine brush. With this method, the size of the collected sample ranged between 1 and 10 μm (LeitzFluovert FS, Leica, Wetzlar, Germany), this being within the range of the mean particle size of the Saharan Desert dust recorded in high-deposition events in the Mediterranean region [*Guieu et al*., 2010]. To avoid any contamination with metals, we previously cleaned the plastic material and glass in contact with the soil using a 0.2 M HCl acid bath and Milli-Q® water.

Previously to the experimental dust addition, P-release experiments at the laboratory showed that 4.1 mg L^{-1} of dust released 0.97 ± 0.17 μM P. We calculated this concentration from the dust weight versus P concentration correlation (r^2: 0.979; *p*-value: 0.029). Thus, adding 61.5 mg of Saharan dust to each microcosm (15 L) resulted in an experimental increase of 0.97 μM of P, mimicking a heavy but still realistic Saharan dust deposition, characteristic for the western Mediterranean region (sea and lakes) [*Morales-Baquero et al*., 2006; *Lekunberri et al*., 2010] and dust concentrations ranging 10–64 g m^{-2} [*Romero et al*., 2011; *Ridame et al*., 2014] during intense intrusion events of atmospheric aerosols over this area.

2.2. Physical Parameters

2.2.1. Radiation Measurements

A multichannel radiometer (Biospherical Instruments Inc., CA, USA), located on the deck of oceanographic ship, continuously registered measurements of the incident radiation at wavelengths representative of the different regions of the solar spectrum (305, 320, and 380 nm and full PAR (400–700 nm)) from the sunrise to sunset during the experimental period (17–21 June 2014). Vertical profiles of radiation attenuation with depth (at the same wavelengths as air measurements) and temperature of water column were determined at noon using a submersible radiometer (Biospherical Instruments Inc., CA, USA). Diffuse attenuation coefficients for downward radiation (k_d) in the upper layers (0 to 10 m) were determined from the slope of the linear regression of the natural logarithm of downwelling irradiance versus depth for each wavelength.

The mean irradiance (Im ((λ)) for the different regions of the solar spectrum (305, 320, and 380 nm and PAR) within the surface upper layers for each area was calculated as in equation (1):

$$\mathrm{Im}(\lambda) = \frac{I_0(\lambda)[1 - \exp(-k_d(\lambda)z)]}{k_d(\lambda)z} \quad (1)$$

where $I_0(\lambda)$ is the mean incident surface irradiance, $k_d(\lambda)$ is the mean attenuation coefficient for different region of the solar spectrum (305, 320, and 380 nm and PAR), and z is the depth of the UML, 2 m in offshore and 6 m in the nearshore.

2.3. Chemical Parameters

Samples for chemical determination of total dissolved N (TDN) and total dissolved P (TDP) were collected daily at each station early in the morning from each microcosm in 300 mL PET bottles and frozen at −20°C until analyzed. Water samples for determining the TDN and TDP were filtered at low pressure (<100 mmHg) using glass-fiber filters (Whatman GF/F, 25 mm diameter). The TDP and TDN concentrations were determined in 25 mL aliquots after digestion with a mixture of potassium persulphate and boric acid at 120°C for 30 min following the spectrophotometric method by *Koroleff* [1977]) with a limit detection of 0.2 μM for N and 0.03 μM for P. To determine sestonic carbon (C), N, and P, volumes of 3 L for C-N or 1.5 L for P were filtered through precombusted (1 h at 550°C) glass-fiber filters (Whatman GF/F, 25 mm diameter). Filters for P, N, and C were immediately frozen at −20°C. In the laboratory, C and N analyses were performed using a Perkin-Elmer 2400 elemental analyzer with a limit detection of 1–3600 μg and 1–6000 μg for C and N, respectively. Determination of sestonic P followed the same method described for TP. Blanks were performed in all procedures. The sestonic N:P ratio was calculated on a molar basis.

For dissolved organic carbon (DOC) determination, samples from each microcosm were filtered through precombusted (2 h at 500°C) glass-fiber filters (Whatman GF/F, 25 mm diameter) and acidified with HCl 1 N (2%). The measurements were made in a total organic carbon analyzer (TOC-VCSH/CSN Shimadzu) with a detection limit of 50 ppb.

2.4. Biological Parameters

2.4.1. Chlorophyll *a* Concentrations and UV-Absorbing Compounds

The Chlorophyll *a* (Chl *a*) concentration was determined by fluorometric technique using the equations of *Jeffrey and Humphrey* [1975]. The samples were filtered onto glass-fiber filters (Whatman GF/F, 25 mm diameter) and the photosynthetic pigments were extracted in 5 mL of absolute methanol for 24 h at 4°C in darkness to remove all the chlorophyll from the filters. The extracts were measured using a fluorometer (Perkin-Elmer model LS 55, Boston, MA, USA). Previously, a calibration curve was made with pure spinach-chlorophyll extract (Sigma Aldrich, USA) to transform fluorescence values into Chl *a* concentration. In addition, the same sample was used to determine UV-absorbing compounds (UV-ACs) by scanning between 250 and 750 nm using a Perkin Elmer UV/VIS spectrophotometer Lambda 45. The resulting scans were processed using a baseline correction, taking in account the whole area under the peak at 337 nm, as well as its height. Owing to the similarities between the two values, the peak height at 337 nm was used as previously described in *Helbling et al*. [1996].

2.4.2. Chlorophyll Fluorescence

Subsamples of 3 mL were taken from each microcosm every 2.5 h over diel cycles to measure in vivo Chl *a* fluorescence using a portable pulse-modulation fluorometer (Water-ED PAM, Walz, Germany). Because the time between sampling and fluorescence measurements was on the order of a few seconds, the intrinsic photochemical efficiency of PSII (Photosystem II, Φ_{PSII}) in the light was determined [*Maxwell and Johnson*, 2000] as equation (2):

$$\Phi_{PSII} = \frac{\Delta F}{F'm} = \frac{F'm - F't}{F'm} \quad (2)$$

where $F'm$ is the instantaneous maximum fluorescence induced by a saturating light pulse (~5300 μmol photons m^{-2} s^{-1} in 0.8 s) and $F't$ is the current steady state fluorescence of light-adapted cells induced by an actinic light ~419 W m^{-2} in light-adapted cells. Each subsample was measured 6 times immediately after sampling, with each measurement lasting 10 s; hence, the total measurement time for each sample was 1 min.

2.4.3. Integral Yield

The Φ_{PSII} integral was calculated from Φ_{PSII} diel cycles (in triplicate for each treatment) following equation (3):

$$A = \int_b^a f(x)dx \quad (3)$$

where *a* and *b* are the initial and final times of measurement for each experimental day, respectively, and *f*(*x*) is the curve describing the yield over time for each treatment. The integral of the curve was calculated utilizing the software MATLAB® r2015a (Mathworks, Natick, Massachusetts, USA) and represents the balance between photoinhibition and repair of PSII throughout the diel cycle.

2.4.4. Nonphotochemical Quenching (NPQ)

The nonphotochemical quenching of Chl *a* fluorescence was used as a proxy of the dissipation of the excess energy as heat and was determined directly using the PAM fluorometer as equation (4):

$$\mathrm{NPQ} = \frac{Fm - F'm}{F'm} \quad (4)$$

where *Fm* is the maximal fluorescence of dark-adapted sample and *F′m* is the instantaneous maximum fluorescence induced by a saturating light pulse (~5300 μmol photons m^{-2} s^{-1} in 0.8 s). The software stored the *Fm* value that was then used with each sample to calculate the NPQ. This is the most important short-term photoprotective mechanism activated by saturating radiation intensities. Because no significant differences were found between NPQ values calculated in this way and those determined from *Fm* measured after an acclimation period in darkness and *F′m* measured during the exposure to radiation, we used the data provided directly by the instrument. For calculating the UVR effect, we used NPQ values registered at noon (T2 in Web repository file—http://hdl.handle.net/10481/46928), corresponding with the moment of maxima inhibition and highest nonphotochemical quenching.

2.4.5. Primary Production

PP was measured by assessing the ^{14}C incorporation by phytoplankton cells [*Steemann Nielsen*, 1952]. Briefly, two sets (one for each marine area) of 16 FEP narrow-mouth Teflon bottles (35 mL, Nalgene; three clear and one dark bottle per treatment) were filled with water from microcosms, inoculated with 5 μCi of labeled sodium bicarbonate (DHI Water and Environment, Germany), and incubated during 4 h centered at noon in tanks under the same conditions as with the microcosms. Then, the content of each bottle was fractionated through to a serial filtration procedure to determine the microplanktonic primary production (PP_M) (cells retained in 3 μm glass-fiber filters, Whatman GF/D, 25 mm diameter) and subsequently the picoplanktonic primary production (PP_P) (cells retained in 0.7 μm Whatman GF/F, 25 mm diameter). To minimize cell breakage, we performed the filtrations at low pressure (<100 mm Hg). Filters were put into 20 mL scintillation vials, acidified with 100 μL of 1 N HCl (2%), and kept open for 24 h in an aeration hood following the recommendations of *Lignell* [1992] to remove DI^{14}C. Finally, 16 mL of scintillation cocktail (Ecoscint A) were added to the vials and counted using a scintillation counter (Beckman LS 6000TA) equipped with autocalibration. Total primary production (TPP) was calculated as the sum of micro(PP_M) and autotrophic picoplanktonic fraction (PP_P).

2.4.6. Abundance, Biomass, Taxonomical Composition, and Net Growth Rates of Autotrophic Picoplankton

Seawater samples from each microcosm were fixed with glutaraldehyde (1% final concentration) and immediately frozen in liquid nitrogen [*Vaulot et al*., 1989]. We took 5 mL subsamples to quantify cell abundance of autotrophic picoplankton (*Prochlorococcus*, *Synechococcus*, and picoeukaryotes) using a Becton Dickinson FACScan flow cytometer (more details in *Mercado et al*. [2006]). Biovolume for these three groups, calculated following *Ribés et al*. [1999] for samples collected in the north-western Mediterranean Sea, were assumed to be 0.18, 0.44, and 1.68 μm^3 for *Prochlorococcus*, *Synechococcus*, and picoeukaryotes, respectively.

The net growth rates (NGR) for each experimental period was calculated according to equation (5):

$$\mathrm{NGR} = \frac{\ln N_t - \ln N_0}{t} \quad (5)$$

where N_t is the cell abundance (cell mL^{-1}) on each experimental day, N_0 is the cell abundance (cell mL^{-1}) at the initial time, and *t* is the time interval between each consecutive experimental day and the initial time. We considered that net growth rate is a good indicator of UVR effect even though some studies have shown that this rate could be influenced by predation effects [*Christaki et al*., 2001].

2.5. Calculations and Statistical Analysis

For the observational study, forward stepwise multiple-regression analyses were carried out to assess the relative influence of potential factors (DOC, temperature, k_{305}, k_{320}, k_{380}, k_{PAR}, TDN, TDP, pH, salinity, conductivity, and TNP:TDP ratio) controlling the distribution of *Synechococcus*, *Prochlorococcus*, picoeukaryotes, and total APP. Linearity and multiorthogonality among independent variables were verified by previous correlation analysis, whereas the normal distribution of residues was checked by Kolmogorov-Smirnov tests. Maps throughout this article were created using ArcGIS® software by Esri (Release 10.4.1. Redlands), and calculations of regional abundance from station points were interpolated using an inverse distance-weighted technique.

T-test analyses were used to determine the differences between marine areas for TDP, TDN, sestonic C, N, and P, DOC, and Chl *a* at initial conditions of the experiment.

The effect size of UVR for each dust treatment and area on Φ_{PSII} integral, NPQ, PP_P, and NGR of *Prochlorococcus*, *Synechococcus*, and picoeukaryotes was calculated as follows in equation (6):

$$\text{Effect size of UVR}\,(\%) = \frac{X_{-\text{UVR}} - X_{+\text{UVR}}}{X_{-\text{UVR}}} \times 100 \tag{6}$$

where X is the variable response considered in samples under the −UVR and +UVR treatments. Error propagation was used to calculate the variance of the UVR effect size (as a percentage). The influence of dust over time on the effect size of UVR on Φ_{PSII}-integral, NPQ, PP_P, and NGR was tested using a one-way repeated measures analysis of variance (one-way RM-ANOVA) for each area. A two-way repeated measures analysis of variance (two-way RM-ANOVA) was used to test the effect of UVR, dust addition, and their interaction over time on Φ_{PSII}-integral, NPQ, PP_P, and *Prochlorococcus*, *Synechococcus*, and picoeukaryotes NGR. The sphericity (by Mauchly's test) and homoscedasticity (by Levene's test) assumptions were verified, and when significant interactive effects were found, differences among and within treatments were assessed by Fisher's least significant differences (LSDs) post-hoc test.

For each response variable, the direction and magnitude of the interactive effect dust × UVR were calculated comparing the values of nonadditive treatment ($+UVR_{Dust}$) with their expected additive value based on the sum of the terms of the individual effects (e.g., (−UVR) + ((+UVR) − (−UVR)) + (($-UVR_{Dust}$) − (−UVR))) following *Piggott et al*. [2015] (in their Figure 2). All tests were performed using Statistica v. 7.0 (Stat Soft, 2007) software.

3. Remote Sensing

The remote-sensing data for the Alboran Sea area were gathered from 1980 to 2015 for the spring-summer (March–September) period. Daily data of the area-average aerosol index (AI) and surface UVR fluxes on this region were downloaded from Giovanni v. 4. 18 3 [*Acker and Leptoukh*, 2007]. The atmospheric dust deposition and UVR fluxes during this season of the year were assessed because both are maximums during this period [see *Morales-Baquero et al*., 2006; *Li et al*., 2015]. AI data were taken from the Total Ozone Mapping Spectrometer (TOMS) Nimbus 7 (21 March 1979 to 5 May 1993), TOMS Earth Probe (22 July 1996 to 21 September 2005), and Ozone Monitoring Instrument (21 March 2006 to 21 September 2015) satellites (data from 1993 to 1996 are not available), while surface UVR-flux data came from the Modern-Era Retrospective analysis for Research and Applications, Version 2, model. Yearly data were used to calculate the mean area average AI and UVR fluxes over the spring-summer period as a measure of the atmospheric dust-deposition intensity and the incidence of UVR fluxes on surface waters.

4. Results

4.1. Dust Deposition and UVR Trends in Alboran Sea

The surface UVR fluxes and, particularly, the AI, exhibited a notable interannual variation (Figure 1). There was a remarkable increase in the AI average intensity, as a measure of the amount of atmospheric aerosol reaching the Alboran Sea throughout the period of 1980–2014, with values ranging between 0.25 (e.g., 1980) and 1.33 (e.g., 2002).

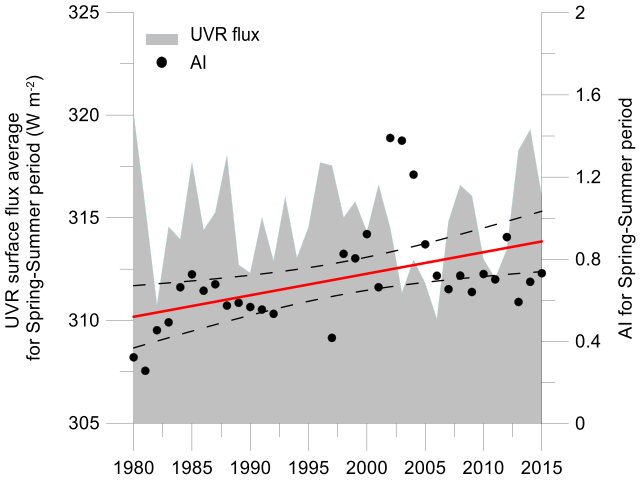

Figure 1. UVR-flux and aerosol index (AI) trend during the 1980–2015 period. The black points represent the area average of AI for the spring-summer period of each year. Linear trend for AI during the studied period is represented through the red line with a positive slope (*y*: 0.01, *x*: −20.24) (*p*-value = 0.046). The grey shaded area shows the surface UVR-flux (in W m^{-2}) from 1980 to 2015.

4.2. Observational Study

Synechococcus, in absolute terms, showed higher abundance values than did the other two picoplanktonic groups throughout the Alboran Sea region (Table S1 in the supporting information). *Prochlorococcus* exhibited the highest abundance values in the central region located between both Gyres, while picoeukaryote organisms increased their presence in the western region of the Alboran Sea, coinciding with the lowest picoprokaryotic abundance (Figure 2). The multiple-regression analysis (Table 1) shows that although total APP abundance positively correlated with TDN concentration, temperature was the main abiotic factor explaining the distribution of each APP group in the Alboran Sea. Thus, temperature positively correlated with *Synechococcus* but negatively with *Prochlorococcus* and picoeukaryotes (Table 1). Accordingly, *Synechococcus* abundance was greater in the warmer eastern region, while *Prochlorococcus* and picoeukaryotes were more abundant in the colder regions (Figure 2). In addition, greater *Prochlorococcus* abundances were associated with high TDN values, whereas picoeukaryote abundances were also higher at low values of salinity (Table 1).

4.3. Experimental Conditions

Penetration of solar radiation into the upper layers of the water column, the daily surface irradiance received by microcosms during the experiments, and vertical profiles of temperature in both areas are shown in Figure 3. The k_d coefficients for each region of the spectrum were low in both areas (<0.5 m^{-1}), indicating high water transparency (Figures 3a and 3b), although the lm (λ) values for the different region of solar spectrum were higher in offshore (Station 3) than nearshore (Station 1) (Table 2). Surface UVR and PAR irradiance reaching the microcosms varied among days (Figure 3c) due to the alternation of cloudy days (19 and 20 June) and sunny days (17, 18, and 21 June). The mean daily irradiance values during the experimental period were 220.2 W m^{-2} for PAR and 0.40, 0.15, and 0.02 W m^{-2} nm^{-1} for the 380, 320, and 305 nm wavelengths, respectively. Surface *T* was higher in the nearshore water column (~17.1°C) than in the offshore (~16.4°C) (Figure 3d). TDP, Chl *a*, and PP_P values were significantly higher in the offshore than in nearshore area (Table 2). These low levels of nutrients in nearshore could indicate that during the sampling period the input of nutrient-rich waters from the sea bottom could be reduced or suppressed. Remarkably, the TDN:TDP ratio was high (920 and 175 for nearshore and offshore, respectively) which also matched the high sestonic N:P ratio (566 and 243 for nearshore and offshore, respectively) found, indicating a severe limitation by P compared to previous data obtained in the same region for the sestonic [*Mercado et al*., 2005] and TDN:TDP ratio [*Ribera D'Alcalà et al*., 2003]. The TDP concentration in the dust-addition treatments declined progressively over the experiment from ~1 μM to concentrations close to 0.4–0.5 μM (Figures S1a and S1b in the supporting information).

4.4. Joint Effects of Dust and UVR in Offshore

From diel cycles of Φ_{PSII} (Figures S2a and S3a), we calculated the UVR effect on the Φ_{PSII} integral, as shown in Figure 4a. The Φ_{PSII} diel cycles exhibited a clearly U-shaped, with lowest Φ_{PSII} at noon and the highest values at the beginning of exposure and at night, after the radiation stress had been removed.

For offshore area, under no-dust conditions, UVR exerted a significant stimulatory effect (except for day 2) on the Φ_{PSII} integral (Figure 4a) with the highest stimulation (i.e., negative values) on day 3 (−118 ± 9.5%)

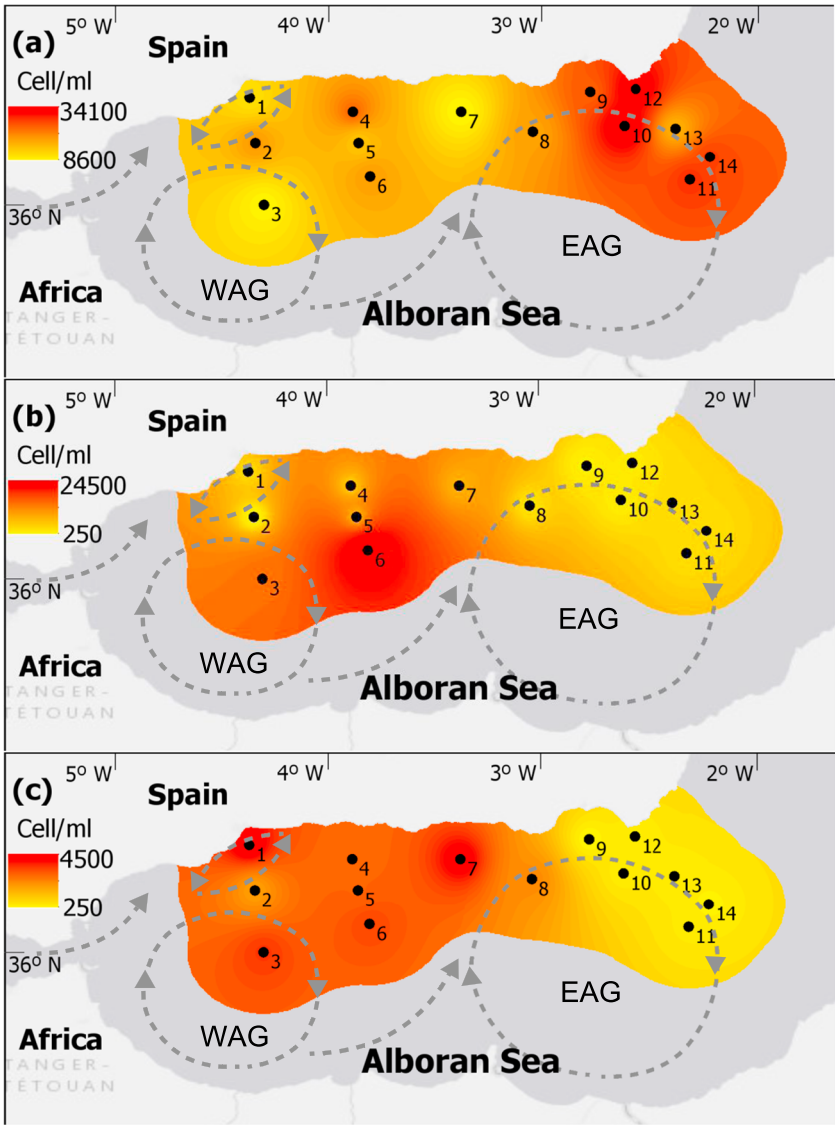

Figure 2. Distribution pattern of (a) *Synechococcus*, (b) *Prochlorococcus*, and (c) picoeukaryote abundances (cells mL^{-1}) throughout the Alboran Sea region. The abundance value for each group and for each station has an area of influence of 20 km. The dotted grey lines represent the Western Anticyclonic Gyre (WAG) and Eastern Anticyclonic Gyre (EAG) and the coastal currents. Note that gyres are represented in relative magnitude and shape. Source: Esri, HERE, DeLorme, MapmyIndia, © OpenStreetMap contributors, and the GIS user community.

Table 1. Results of Multiple Forward Stepwise Regression Analysis for *Synechococcus*, *Prochlorococcus*, Picoeukaryotes, and Total Autotrophic Picoplankton Abundances of the 14 Stations Analyzed

Dependent Variable	Independent Variable	Beta	Multiple R^2	R^2 Exchange	*p*
Synechococcus abundance	Temperature	0.628	0.49	0.49	0.02
Prochlorococcus abundance	TDN	0.805	0.43	0.43	0.03
	Temperature	−0.743	0.74	0.30	0.02
Picoeukaryotes abundance	Temperature	−0.423	0.76	0.76	<0.001
	Salinity	−0.594	0.87	0.11	0.03
Total APP	TDN	0.759	0.58	0.58	<0.01

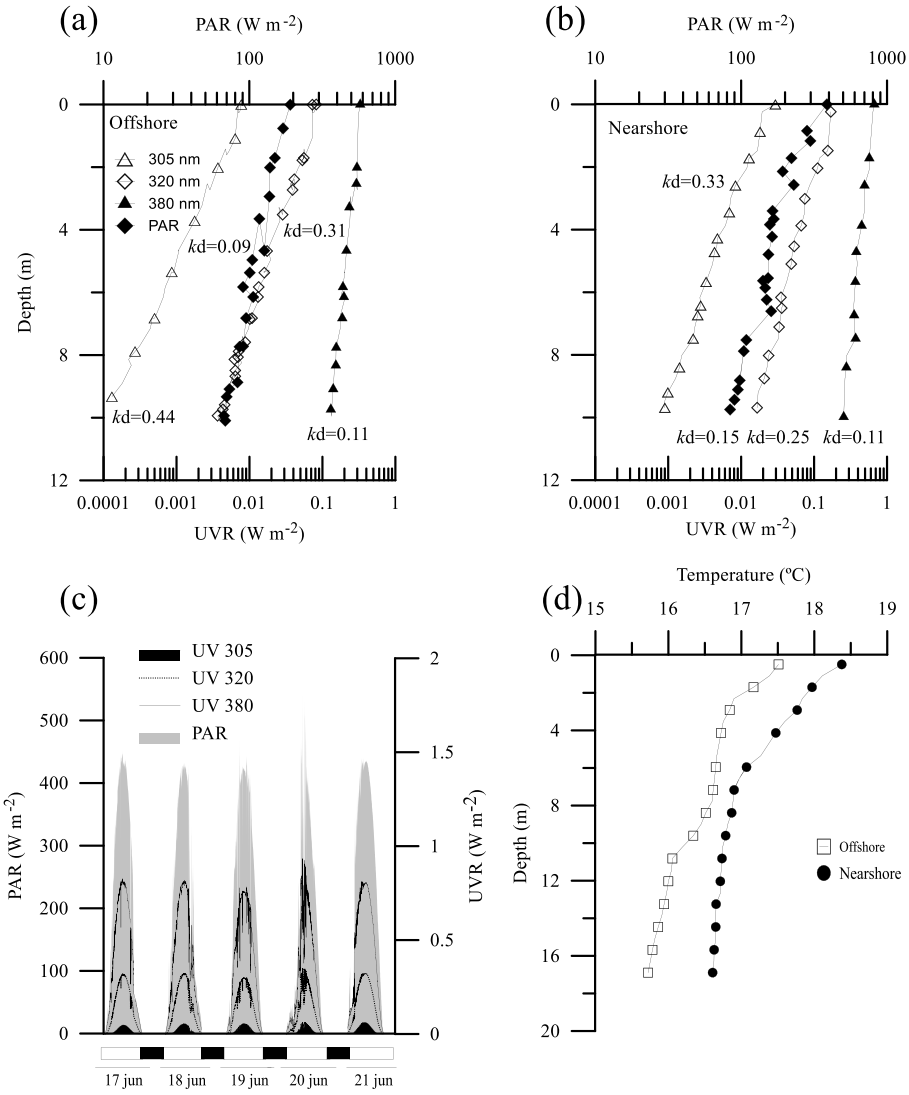

Figure 3. Vertical profiles of radiation and diffuse attenuation coefficients (k_d) into the water column of (a) offshore and (b) nearshore for 305, 320, and 380 nm and PAR are shown. (c) Surface solar radiation for PAR and 305, 320, and 380 of wavelength for UVR over microcosms in the Alboran region during the exposure time (17–21 June 2014) and (d) vertical profiles of temperature into the water column are also shown.

and at the end of the experiment (−88 ± 33% on day 5). Under the dust treatments the opposite pattern was found, as UVR significantly inhibited the Φ_{PSII} integral throughout the experiment (except the first day, −16 ± 1.4%). Hence, a significant dust × time effect was found (Table 3) and the dust × UVR effect shifted from positive antagonism over the short term (i.e., dust diminished UVR damage; Table 4) to negative synergism (i.e., dust accentuated UVR damage; Table 4), with the lowest Φ_{PSII} integral at the end of the experiment.

Because the biological meaning of the NPQ variable coping with UVR stress was opposite to that of the other variables analyzed in our experiment, a positive value of the UVR effect on NPQ means low stress by UVR, as opposed to the other variables, where a positive value signifies an inhibitory UVR effect (see Figure 4). Over the short term, NPQ values were low under UVR, and therefore, UVR stimulated the NPQ variable (+100 ± 0.75%; Figure 4b) regardless of dust addition. However, at the end of the experiment (day 5) a dual response was found: under no-dust conditions UVR exerted a stronger inhibitory effect on NPQ, increasing its value (−47.5%), whereas under dust addition the stimulatory effect of UVR significantly decreased (+29.5 ± 7.3) (Figure 4b).

Table 2. Values of Physical, Chemical, and Biological Conditions at the Initial of the Experiment in Offshore and Nearshore in Alboran Sea[a]

Variable	Offshore	Nearshore	*p*
Im_{305} (W m^{-2})	0.019	0.013	
Im_{320} (W m^{-2})	0.185	0.138	
Im_{380} (W m^{-2})	0.689	0.574	
Im_{PAR} (W m^{-2})	536.3	394.4	
TDP (μM P)	0.54 ± 0.012	0.10 ± 0.005	**<0.001**
TDN (μM N)	95 ± 26	92 ± 10	0.86
TDN:TDP ratio	175 ± 52	920 ± 146	**<0.01**
DOC (μM C)	213 ± 31	321 ± 89	0.12
Chl *a* (μg L^{-1})	1.80 ± 0.25	0.80 ± 0.09	**<0.01**
Sestonic N (μM N)	4.38 ± 0.47	8.49 ± 0.45	**<0.001**
Sestonic P (μM P)	0.02 ± 0	0.01 ± 0	**<0.001**
Sestonic N:P ratio	243 ± 30	566 ± 32	**<0.01**
Algal biomass (μg C L^{-1})	120 ± 4	55.7 ± 0.2	**<0.001**
PP_P (μg C L^{-1} h^{-1})	6.26 ± 1.17	1.33 ± 0.41	**<0.01**
PP_P: Chl *a*	3.29 ± 0.01	1.77 ± 0.01	**<0.001**

[a]Values of mean irradiances (Im (λ)) for different regions of the solar spectrum (305, 320, and 380 nm and photosynthetically active radiation (PAR, 400–700 nm)) are shown. Mean (±SD) concentrations of total dissolved phosphorous (TDP) and nitrogen (TDN), dissolved organic carbon (DOC), chlorophyll *a* (Chl *a*), sestonic N, P, algal biomass (C), sestonic N:P ratio, picoplanktonic primary production (PP_P), and PP_P:Chl *a* ratio. The numbers in bold indicate *p*-values <0.05.

TPP values ranged from 3.5 to 12 mg C m^{-3} h^{-1} for different treatments over the experiment. Because more than 90% of TPP was due to APP fraction (Figure S2b), we focused the analysis on this fraction. In the offshore (Figure 4c), UVR exerted a significant impact on PP_P over the incubation period, shifting from inhibitory to stimulatory effect under the no-dust treatment (from +15.7 to −41.8 values) and from stimulatory to inhibitory effect under the dust treatment (from −93.6 to +31.5 values). Thus, the dust × UVR effect changed from positive synergistic at short term to negative synergistic effect at the end of the experiment (Table 4), showing a response pattern similar to that of Φ_{PSII} integral at day 5.

Biovolumes of the different APP organisms in the offshore area varied from 250 μm^3 mL^{-1} for *Prochlorococcus* to 3000 μm^3 mL^{-1} for *Synechococcus* and 6000 μm^3 mL^{-1} for picoeukaryotes at the beginning of the experiment; contrarily, the biovolume fell for picoeukaryotes and *Synechococcus* but rose for *Prochlorococcus* over the experiment (Figures S2c–S2e).

For picoeukaryotes, the NGR was not significantly affected by UVR over the short term regardless of the dust treatment (Figure 4d). However, toward the end of the experiment, UVR exerted a significant stimulatory effect under no-dust conditions, but inhibitory under dust addition. Hence, dust × UVR changed from positive antagonism to negative synergism (Table 4). This response pattern is similar to that observed for the Φ_{PSII} integral and PP_P (Table 4). However, the NGR response of *Synechococcus* was different (Figure 4e) because under no-dust conditions, UVR exerted a stimulatory effect throughout the experiment. Nevertheless, dust addition altered the UVR effect over time (Table 3) from inhibitory (negative synergism) over short term to stimulatory (positive synergism) toward the end of the experiment (Table 4). The NGR of *Prochlorococcus* showed no clear response under no-dust conditions (Figure 4f). However, as in the case of picoeukaryotes, dust addition significantly shifted the initial stimulatory (positively synergistic) UVR effect to inhibitory (negatively synergistic) toward the end of the experiment (Table 4).

4.5. Joint Effects of Dust and UVR in the Nearshore Area

For the nearshore area, under no-dust conditions, UVR exerted a clear inhibitory effect on the Φ_{PSII} integral (except for day 2; Figure 5a). However, dust addition gradually transformed the inhibitory effect to a stimulatory one over experimental time (−20.1 ± 5.9% on day 5) (significant dust × time; Table 3). Hence, dust × UVR effect ranged from negative synergism (i.e., dust accentuated the inhibitory UVR effect) over the short term to negative antagonism (i.e., dust reversed the inhibitory UVR effect) toward the end of the experiment (see Table 4).

The UVR effect on NPQ is shown in Figure 5b. Under the no-dust conditions, UVR raised NPQ values, exerting a significant inhibitory effect (−44.9 ± 10.8%). This UVR effect was attenuated over the experiment. Dust addition spurred the initial inhibitory UVR effect on NPQ (−99 ± 9.3%), although the effect significantly weakened toward the end of the experiment (16.4 ± 6.7%) (Table 3), which matched the inverse pattern observed in the Φ_{PSII} integral.

TPP values increased from 1 at the beginning of the experiment to 11 mg C m^{-3} h^{-1}on the 21 June. As for the offshore, the APP fraction (<3 μm) in nearshore also represented about 90% of the TPP (Figure S3b). Under no-dust conditions, UVR inhibited PP_P (16.5 ± 6.1%) over the short term but stimulated it (−89.7 ± 15.7%) at

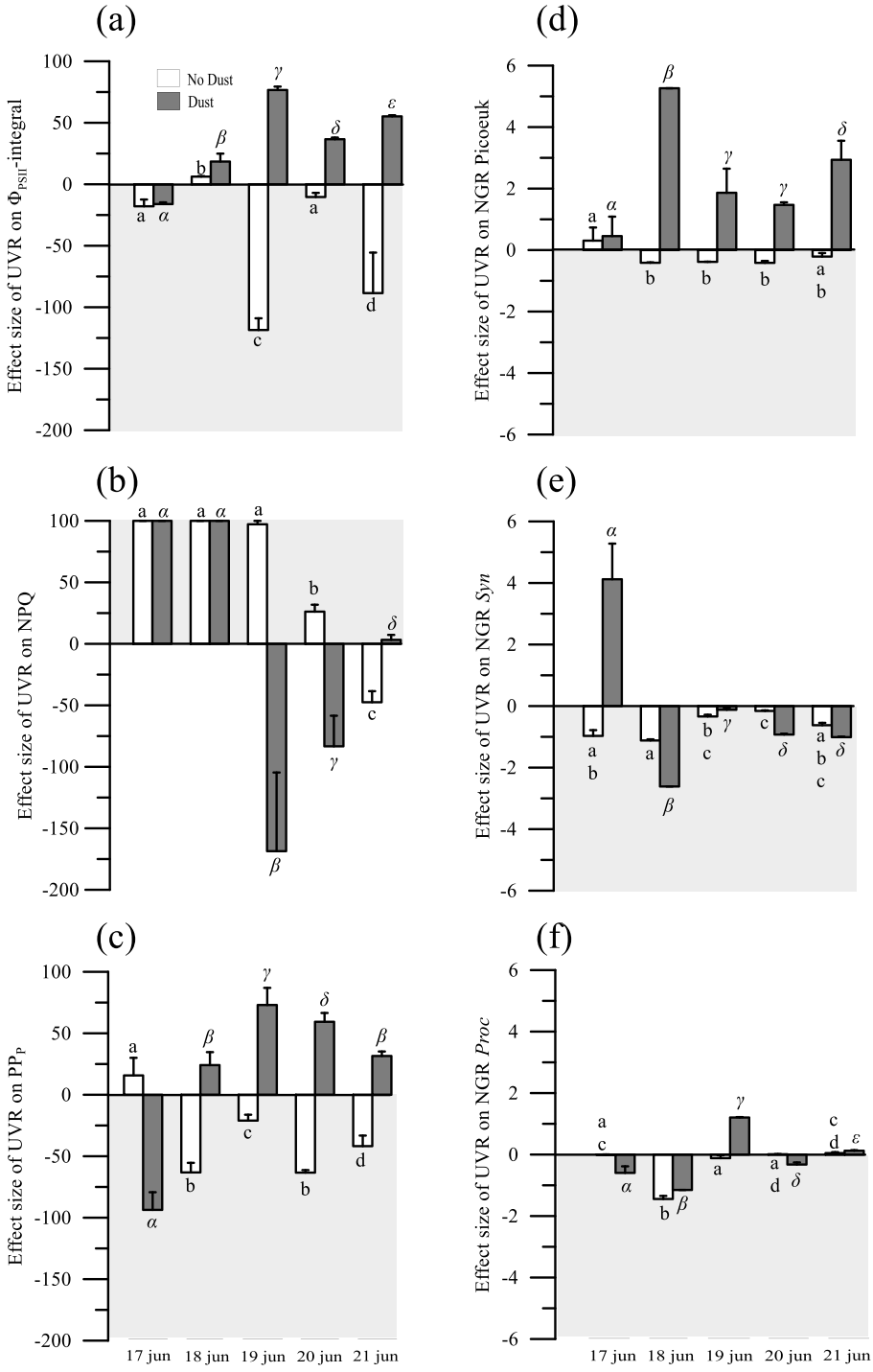

Figure 4. Effect size of UVR on (a) photosynthetic quantum yield (Φ_{PSII} integral), (b) nonphotochemical quenching (NPQ), (c) picoplanktonic primary production (PP_P), and net growth rate (NGR) for (d) picoeukaryotes (Picoeuk), (e) *Synechococcus* (*Syn*), and (f) *Prochlorococcus* (*Proc*) from offshore. The shaded area represents stimulatory effect. Each bar represents the mean values of three replicates, while the vertical lines indicate the standard deviation. The italic letters indicate differences among no-dust treatment, whereas the Greek letters indicate differences among dust treatment by LSD post-hoc test over the experiment.

the end of the experiment (Figure 5c). By contrast, under the dust addition, UVR stimulated PP_P over the short term (−75.4 ± 16.7%) but inhibited it over the experiment (−24.9 ± 27.2% on day 5), hence prompting a change in the interaction between the two factors from negative to positive antagonism (Table 4).

Table 3. Results of the One-Way RM-ANOVA of Dust Addition on Effect Size of UVR on Photosynthetic Quantum Yield (Φ_{PSII} Integral), Nonphotochemical Quenching (NPQ), Picoplanktonic Primary Production (PP_P), and Net Growth Rate (NGR) for Picoeukaryotes (Picoeuk), *Synechococcus* (*Syn*), and *Prochlorococcus* (*Proc*) From Offshore and Nearshore Areas[a]

		Φ_{PSII} Integral		NPQ		PP_P		NGR Picoeuk		NGR *Syn*		NGR *Proc*	
Effect	d.f.	*F*	*p*	*F*	*p*	*F*	*p*	*F*	*p*	*F*	*p*	*F*	*p*
						Offshore							
Dust	1	340.5	**<0.001**	26.7	**<0.01**	55.6	**<0.01**	294.7	**<0.001**	0.6	**<0.05**	3.6	**<0.01**
Dust × time	4	87.8	**<0.001**	73.6	**<0.001**	617.5	**<0.001**	73.5	**<0.001**	9.8	**<0.001**	9.3	**<0.001**
						Nearshore							
Dust	1	8.5	0.14	0.00	0.97	4.5	0.10	7.81	0.07	79.6	**<0.01**	0.01	0.95
Dust × Time	4	12.8	**<0.001**	36.7	**<0.001**	185.9	**<0.001**	14.2	**<0.01**	32.5	**<0.001**	44.3	**<0.001**

[a]Significant *p*-values are typed in bold. d.f. represents the degree of freedom and *F* the *F* test.

APP biovolumes are represented in Figures S3c–S3e. At initial conditions, biovolumes for picoeukaryotes (7500 μm^3 mL^{-1}) and *Synechococcus* (5300 μm^3 mL^{-1}) were higher than in the offshore, whereas the *Prochlorococcus* biovolume was lower (100 μm^3 mL^{-1}) than in the offshore. Nevertheless, as in the offshore, biovolumes showed a generalized decline for picoeukaryotes and *Synechococcus* but a surge for *Prochlorococcus* over the experiment.

APP showed different responses to UVR depending on the APP group. Thus, an inhibitory UVR effect on NGR of picoeukaryotes declined over the experimental time, being more accentuated under no-dust conditions (Figure 5d). By contrast, the NGR of *Synechococcus* was stimulated by UVR at short term (-0.65 ± 0.07 on day 2) but inhibited significantly at the end of the experiment (0.18 ± 0.08) under no-dust conditions (Figure 5e). However, under dust addition, UVR significantly stimulated the NGR of *Synechococcus* over the experiment, generating an antagonistic dust × UVR effect (Table 4). *Prochlorococcus* failed to show a clear response, except for a significant UVR-inhibition on intermediate days (day 2, under no-dust addition; days 2 and 3 under dust addition; Figure 5f).

5. Discussion

Our observational results indicate that temperature was the common regulating factor of distribution for each APP group in early summer, and that nutrients, mainly TDN, determined the total abundance of APP throughout the Alboran Sea. Although picoeukaryotes and *Prochlorococcus* showed a greater preference for colder western water, *Synechococcus* was the most dominant group in the region (except at stations 1, 3, and 7, dominated by picoeukaryotes). This was probably because the P-limited conditions of Alboran Sea, and their lower demand of P, favored them with respect to picoeukaryotes [*Stawiarski*, 2014]. A global picoplankton distribution pattern determined by temperature, and, in agreement with our results, has been mentioned by *Buitenhuis et al*. [2012]. In addition, the total APP abundance was slightly higher in the warmer eastern region of Alboran Sea, coinciding with the highest TDN. These results agree with those found by *Amorim et al*. [2016] in this area and by *Moore et al*. [2008] in the oligotrophic subtropical North Atlantic Ocean, showing APP development with increasing N sources.

The predicted rising of water temperature funneled by global climate change will promote the stratification of the water column, causing thinner UML and exposing phytoplankton to higher levels of visible and UVR [*Peralta-Ferriz and Woodgate*, 2015]. Additionally, as a consequence of the stronger stratification, the nutrient supply to surface waters from deep mixing will become increasingly low, causing other nutrient sources such as atmospheric dust to acquire a more relevant role as a modulator of the phytoplankton dynamics. Therefore, our experimental approach can be considered representative of these expected conditions of global warming because the water column was already relatively stratified, possibly explaining the low nutrient concentration found in the UML. Moreover, the experimental exposure of the samples to UVR under a relatively thin layer of water simulated the expected shallower UML (i.e., representing the worst scenario of radiation exposure), predicted under global warming. Given the enormous importance of APP on microbial food web structure and functioning of the Alboran Sea, our experimental approach fills a gap of knowledge on how the interaction of these two main factors of global change affects physiology, metabolism, and taxonomical composition of APP. The experimental design allowed us to infer that the response patterns

Journal of Geophysical Research: Biogeosciences 10.1002/2017JG003834

Table 4. Short-Term and Midterm Effects of UVR, Dust, and Magnitude and Direction of the UVR × Dust Interaction (Nonadditive) Over the Experiment for Offshore and Nearshore on Photosynthetic Quantum Yield (Φ_{PSII} Integral), Nonphotochemical Quenching (NPQ), Picoplanktonic Primary Production (PP_P), and Net Growth Rate (NGR) for Picoeukaryotes (Picoeuk), *Synechococcus* (*Syn*), and *Prochlorococcus* (*Proc*)[a]

		Short-Term Effect							Midterm Effect						
		Control	UVR	Dust	Add	Nonadd	Int.	B.M.	Control	UVR	Dust	Add	Nonadd	Int.	B.M
Offshore	Φ_{PSII} integral	3.01	3.68	3.22	3.89	3.75	**+A**	Stimulation	1.76	3.31	3.27	4.82	1.47	**−S**	Inhibition
	NPQ	0.006	0	0.001	0	0	**−S**	Stimulation	29.26	43.16	26.4	40.26	25.51	**−S**	Stimulation
	PPp	8.17	6.89	5.79	4.51	11.21	**+S**	Stimulation	7.17	10.17	10.14	13.14	6.94	**−S**	Inhibition
	NGR Picoeuk	−0.38	−0.5	−0.29	−0.41	−0.43	**+A**	Inhibition	−0.35	−0.28	−0.15	−0.08	−0.57	**−S**	Inhibition
	NGR *Syn*	−0.21	−0.006	−0.12	0.084	−0.60	**−S**	Inhibition	−0.55	−0.21	−0.46	−0.12	0.005	**+S**	Stimulation
	NGR *Proc*	−1.513	−1.510	−1.66	−1.657	−0.67	**+S**	Stimulation	0.22	0.21	0.199	0.189	0.17	**−S**	Inhibition
Nearshore	Φ_{PSII} integral	3.29	3.02	2.42	2.15	2.12	**−S**	Inhibition	2.98	2.63	2.63	2.28	2.76	**−A**	Stimulation
	NPQ	0.898	1.30	0.596	0.998	1.19	**+A**	Inhibition	41.01	41.89	30.83	31.71	25.77	**−S**	Stimulation
	PPp	4.80	4.01	1.51	0.72	2.64	**−A**	Stimulation	4.86	9.21	8.02	12.37	10.01	**+A**	Stimulation
	NGR Picoeuk	−0.45	−0.92	−1.66	−2.13	−1.97	**−A**	Inhibition	−0.31	−0.35	−0.32	−0.36	−0.28	**+S**	Stimulation
	NGR *Syn*	−0.16	−0.18	−1.24	−1.26	−0.61	**−A**	Stimulation	−0.36	−0.42	−0.63	−0.69	−0.40	**−A**	Stimulation
	NGR *Proc*	−1.08	−0.77	−1.14	−0.83	−1.21	**−S**	Inhibition	0.35	0.36	0.29	0.30	0.26	**−S**	Inhibition

[a]Classification of the UVR × dust interaction, following *Piggott et al*. [2015], is positive synergistic (+S), negative synergistic (−S), positive antagonistic (+A), and negative antagonistic (−A). Additive effect and nonadditive effect are abbreviated as add and nonadd, respectively, and the interaction and the biological meaning as Int. and B.M.

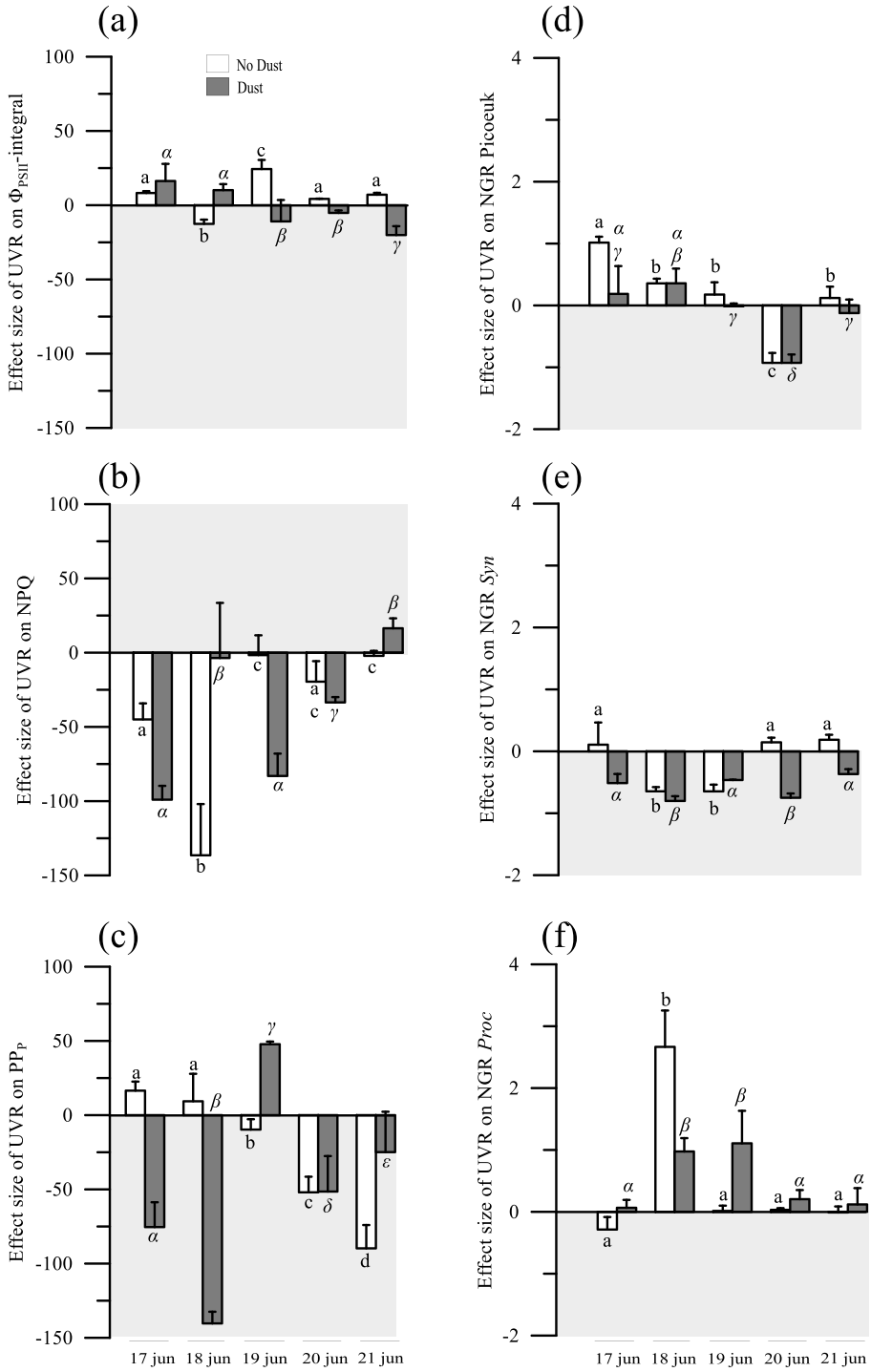

Figure 5. Effect size of UVR on (a) photosynthetic quantum yield (Φ_{PSII}-integral), (b) nonphotochemical quenching (NPQ), (c) picoplanktonic primary production (PP_P), and net growth rate (NGR) for (d) picoeukaryotes (Picoeuk), (e) *Synechococcus* (*Syn*), and (f) *Prochlorococcus* (*Proc*) from nearshore. The shaded area represents stimulatory effect. Each bar represents the mean values of three replicates, while the vertical lines indicate the standard deviation. The italic letters indicate differences among no-dust treatment, whereas the Greek letters indicate differences among dust treatment by LSD post-hoc test over the experiment.

observed in the picoplanktonic community of each region were due to the effects of the two factors experimentally assayed (UVR and dust), since the conditions to which the microcosms were exposed were identical for all experimental units.

According to our hypothesis, UVR under ambient (no-dust) conditions exerted a stronger inhibitory effect on most of variables measured in nearshore than in offshore over both short-term and midterm (day 5) temporal scales. Moreover, it was remarkable that in offshore, UVR stimulated photosynthetic variables (Φ_{PSII} integral and PP_P) throughout the experiment, indicating a great photoacclimation of picoplanktonic communities to high UVR exposure. This finding could be explained by the differential previous light history of communities, implying different acclimations between the two areas studied. In fact, the picoplanktonic community in the offshore was subjected to higher mean irradiances of UVR and PAR owing to a shallower UML (2 m) than in the nearshore (6 m), which could favor a higher photoacclimation in the former area when the picoplankton was exposed to our experimental conditions. Additionally, this greater acclimation of the offshore picoplankton could be supported by the higher PP_P:Chl *a* ratio (≈2-fold) found [*Thomas et al*., 1992] (see Table 2), as well as by the lower NPQ values found, which may be related to the absence of a chronic damage in the photosynthetic apparatus [*Krause and Weis*, 1991; *Cruz and Serôdio*, 2008]. Nevertheless, based on our results, we cannot rule out a stimulatory UV-A effect on photosynthesis, as reported by *Barbieri et al*. [2002] and *Gao et al*. [2007]. Moreover, the contrasting sensitivity to UVR of both communities in their photosynthetic, metabolic, and structural variables may also be the consequence of their previous nutritional state [*Winder*, 2009; *Romero et al*., 2011; *Helbling et al*., 2013] basically, a noticeably higher P limitation in the nearshore, because we found no difference in DOC concentrations between the two areas to explain their different UVR sensitivity (Figures S4a and S4b).

Notably, and partially contrary to our hypothesis, the addition of Saharan dust had a contrasting effect on the photosynthetic activity and C incorporation of the picoplanktonic communities from nearshore versus offshore. In nearshore, the harmful UVR effect was inverted to stimulatory by dust addition at the end of the experiment. This stimulation was promoted from the subcellular level (Φ_{PSII} integral), through metabolism (PP_P), to the community level, as the responses (NGR) of picoeukaryotes and *Synechococcus* sp. Moreover, in the absence of significant UV-AC concentration over the experiment (data not shown) to cope with the UVR damage [*Sinha and Häder*, 2008], the increase in the Φ_{PSII} integral and the photoacclimation of the communities together with a progressively declining NPQ activity demonstrate a lesser need to dissipate the excess of energy absorbed by PSII, hence supporting the idea of an improved physiological state under UVR after dust addition. Curiously, a similar positive effect of UVR and nutrient enrichment (P, mimicking similar dust inputs as in our study) on PSII and PP_P from the nearshore waters of Alboran Sea has recently been reported by *Sobrino et al*. [2014] and *Carrillo et al*. [2015a], respectively.

By contrast, the negative synergistic dust × UVR effect reported for most of the variables in the offshore suggests a simultaneous constraint exerted after dust addition on the Φ_{PSII}, PP_p, and growth of picoeukaryotes and *Prochlorococcus*, because UVR without dust treatments led to the highest stimulation of all processes (see Table 4). The NPQ photoprotective mechanism also showed a different pattern in the offshore. Thus, the increasing stimulatory UVR effect on NPQ under dust addition over the experiment makes a higher degree of stress evident. This unmasking of a harmful UVR effect on PP and productivity after nutrient enrichment has been widely reported in oligotrophic freshwater [*Carrillo et al*., 2008; *Korbee et al*., 2012; *Durán et al*., 2016] as well as in coastal ecosystems [*Carrillo et al*., 2015a]. Furthermore, this negative synergistic effect on APP could be related to higher rates of DNA synthesis due to stimulated growth induced by the addition of dust rich in limiting nutrients. This can exacerbate the damage of UVR on DNA, increasing the effects of UVR on cell division after addition of dust [*Karentz et al*., 1991].

Our findings also showed general UVR damage on APP biovolume (Figures S2c–S2e and S3c–S3e) over the short term, in agreement with other authors [*Llabrés and Agustí*, 2006], even after dust addition in both areas. However, at the end of the experiment, *Prochlorococcus* was the only fraction that showed a slightly positive development. This finding may be explained by a higher ability of *Prochlorococcus* to grow under P-limitation conditions, which may be accentuated by the supply of nitrogen contained in the dust [*Chien et al*., 2016].

According to the picoeukaryote predominance in total APP biovolume of these two stations, it is not surprising that the physiological state of the community was driven fundamentally by them. Thus, picoeukaryote NGR showed a pattern similar to that of the physiological variables, growing in the nearshore (positive synergism) and exhibiting more severe damage and inhibition in the offshore (negative synergism) at the end of the experiment. However, although the influence of *Synechococcus* on physiological

variables was not notable, probably due to its lower abundance at the beginning of the experiment, it was the only group that showed a consistent positive response under UVR × dust conditions in the two areas studied. It is probable that *Synechococcus* can gain a greater advantage, not only at low P conditions (observational study) but also under the UVR × dust interaction, as have been already demonstrated by *Mackey et al*. [2009], who reported greater positive changes in C biomass of *Synechococcus* after nutrient enrichment at high light intensities.

6. Conclusions

The most striking results of our study were that the joint action of UVR and dust constrained the photosynthesis (Φ_{PSII}-integral and PP_p) and growth rates of the main picoplanktonic groups over time in the offshore. These results call into question the absence of response [*Ridame et al*., 2014] or the widely reported positive dust effect on productivity in open deep-sea areas (i.e., Mediterranean Sea and North and South Atlantic Ocean) through experimental [*Pulido-Villena et al*., 2008; *Marañón et al*., 2010; *Giovagnetti et al*., 2013] and observational studies [*Gallisai et al*., 2014] when the UVR effects are not directly considered. On the other hand, during our observational study, we found that *Synechococcus* represented a high proportion of picoplanktonic community, and our experimental study confirmed that these organisms possess a greater acclimation capacity to new environmental conditions. Therefore, interactions between dust inputs and UVR not only could unravel a contrasting sensitivity of nearshore and offshore picoplanktonic communities from oligotrophic ecosystems but could also suggest that the interaction between these two global-change factors under anticipated future conditions in the Mediterranean region may alter the microbial web structure and functioning of these areas by favoring the greater APP growth, especially of picoprokaryotes. This study underscores the need to know whether the responses of similar organisms can be observed in other oceanic regions conditioned by the presence of gyres that determine different physico-chemical conditions for nearshore and offshore.

Acknowledgments

This study was supported by Ministerio Economía y Competitividad and Fondo Europeo de Desarrollo Regional (FEDER) (CGL2011-23681/BOS and CGL2015-67682-R). We acknowledged Eulogio Corral for his help and cooperation in performing the experiments. Ismael Lopez is acknowledged for having performed cytometry analysis and Jesús M. Mercado for providing us the CTD device. We appreciate the Editor Miguel Goni and two anonymous reviewers for their interesting contribution and comments on early drafts of our manuscript. We also thank the crew of the Oceanographic Ship Francisco de Paula Navarro for the logistic support and David Nesbitt for English-writing assistance. M.J.C. was supported by the Spanish Government Fellowship "Formación de Profesorado Universitario" (FPU12/01243) and by a postdoctoral contract "Contrato Puente" funded by University of Granada (FP7/2017) and METAS project (CGL2015-67682-R). J.M.G.O was supported by the Spanish Government Fellowship "Formación de Profesorado Universitario" (FPU14/00977). Original data from this paper are freely available in the Digibug database (http://hdl.handle.net/10481/46928).

References

Acker, J. G., and G. Leptoukh (2007), Online analysis enhances use of NASA Earth science data, *Eos Trans. AGU*, *88*, 2, doi:10.1029/2007EO020003.

Agawin, N. S. R., C. Duarte, and S. Agustí (2000), Nutrient and temperature control of the contribution of picoplankton to phytoplankton biomass and production, *Limnol. Oceanogr.*, *45*, 591–600, doi:10.4319/lo.2000.45.3.0591.

Agustí, S., and M. Llabrés (2007), Solar radiation-induced mortality of marine pico-phytoplankton in the oligotrophic ocean, *Photochem. Photobiol.*, *83*, 793–801, doi:10.1111/j.1751-1097.2007.00144.x.

Alvain, S., C. Moulin, Y. Dandonneau, and F. M. Bréon (2005), Remote sensing of phytoplankton groups in case 1 waters from global SeaWiFS imagery, *Deep Sea Res., Part I*, *52*, 1989–2004, doi:10.1016/j.dsr.2005.06.015.

Amorim, A. L., P. León, J. M. Mercado, D. Cortés, F. Gómez, S. Putzeys, S. Salles, and L. Yebra (2016), Controls of picophytoplankton abundance and composition in a highly dynamic marine system, the Northern Alboran Sea (Western Mediterranean), *J. Sea Res.*, *112*, 13–22, doi:10.1016/j.seares.2016.02.005.

Báez, J. C., L. Gimeno, M. Gómez-Gesteira, F. Ferri-Yáñez, and R. Real (2013), Combined effects of the Arctic Oscillation and the North Atlantic Oscillation on sea surface temperature in the Alborán Sea, *PLoS One*, *8*(4), e62201, doi:10.1371/journal.pone.0062201.

Barbieri, E. S., V. E. Villafañe, and E. W. Helbling (2002), Experimental assessment of UV effects upon temperate marine phytoplankton when exposed to variable radiation regimes, *Limnol. Oceanogr.*, *47*, 1648–1655, doi:10.4319/lo.2002.47.6.1648.

Behrenfeld, M. J., et al. (2009), Satellite-detected fluorescence reveals global physiology of ocean phytoplankton, *Biogeosciences*, *6*, 779–794, doi:10.5194/bg-6-779-2009.

Belkin, I. M. (2009), Rapid warming of large marine ecosystems, *Prog. Oceanogr.*, *81*, 207–213, doi:10.1016/j.pocean.2009.04.011.

Buitenhuis, E. T., et al. (2012), Picophytoplankton biomass distribution in the global ocean, *Earth Syst. Sci. Data*, *4*, 37–46, doi:10.5194/essd-4-37-2012.

Buitenhuis, E. T., et al. (2013), MAREDAT: Towards a world atlas of MARine Ecosystem DATa, *Earth Syst. Sci. Data*, *5*, 227–239, doi:10.5194/essd-5-227-2013.

Bullejos, F. J., P. Carrillo, M. Villar-Argaiz, and J. M. Medina-Sánchez (2010), Roles of phosphorus and ultraviolet radiation in the strength of phytoplankton-zooplankton coupling in a Mediterranean high mountain lake, *Limnol. Oceanogr.*, *55*, 2549–2562, doi:10.4319/lo.2010.55.6.2549.

Buma, A. G. J., E. W. Helbling, M. K. De Boer, and V. E. Villafañe (2001), Patterns of DNA damage and photoinhibition in temperate South-Atlantic picophytoplankton exposed to solar ultraviolet radiation, *J. Photochem. Photobiol., B*, *62*, 9–18, doi:10.1016/S1011-1344(01)00156-7.

Buma, A. G. J., P. Boelen, and W. H. Jeffrey (2003), UVR-induced DNA damage in aquatic organisms, in *UV Effects in Aquatic Organisms and Ecosystems*, edited by E. W. Helbling and H. E. Zagarese, pp. 291–327, The Royal Society of Chemistry, Cambridge, U. K.

Cabrerizo, M. J., J. M. Medina-Sánchez, J. M. González-Olalla, M. Villar-Argáiz, and P. Carrillo (2016), Saharan dust inputs and high UVR levels jointly alter the metabolic balance of marine oligotrophic ecosystems, *Sci. Rep.*, *6*, 35892, doi:10.1038/srep35892.

Carrillo, P., J. A. Delgado-Molina, J. M. Medina-Sánchez, F. J. Bullejos, and M. Villar-Argáiz (2008), Phosphorus inputs unmask negative effects of ultraviolet radiation on algae in a high mountain lake, *Global Change Biol.*, *14*, 423–439, doi:10.1111/j.1365-2486.2007.01496.x.

Carrillo, P., J. M. Medina-Sánchez, C. Durán, G. Herrera, V. E. Villafañe, and E. W. Helbling (2015a), Synergistic effects of UVR and simulated stratification on commensalistic phytoplankton-bacteria relationship in two optically contrasting oligotrophic Mediterranean lakes, *Biogeosciences*, *12*, 697–712, doi:10.5194/bg-12-697-2015.

Carrillo, P., J. M. Medina-Sánchez, G. Herrera, C. Durán, M. Segovia, D. Cortés, S. Salles, N. Korbee, F. L. Figueroa, and J. M. Mercado (2015b), Interactive effect of UVR and phosphorus on the coastal phytoplankton community of the Western Mediterranean Sea: Unravelling eco-physiological mechanisms, *PLoS One*, *10*(11), e0142987, doi:10.1371/journal.pone.0142987.

Chien, C. T., K. R. M. Mackey, S. Dutkiewicz, N. M. Mahowald, J. M. Prospero, and A. Paytan (2016), Effects of African dust deposition on phytoplankton in the western tropical Atlantic Ocean off Barbados, *Global Biogeochem. Cycles*, *30*, 716–734, doi:10.1002/2015GB005334.

Christaki, U., A. Giannakourou, F. Van Wambeke, and G. Grégori (2001), Nanoflagellate predation on auto- and heterotrophic picoplankton in the oligotrophic Mediterranean Sea, *J. Plankton Res.*, *23*, 1297–1310, doi:10.1093/plankt/23.11.1297.

Cruz, S., and J. Serôdio (2008), Relationship of rapid light curves of variable fluorescence to photoacclimation and non-photochemical quenching in a benthic diatom, *Aquat. Bot.*, *88*, 256–264, doi:10.1016/j.aquabot.2007.11.001.

Day, T. A., and P. J. Neale (2002), Effects of UV-B radiation on terrestrial and aquatic primary producers, *Annu. Rev. Ecol. Syst.*, *33*, 371–396, doi:10.1146/annurev.ecolsys.33.010802.150434.

Durán, C., J. M. Medina-Sánchez, G. Herrera, and P. Carrillo (2016), Changes in the phytoplankton-bacteria coupling triggered by joint action of UVR, nutrients, and warming in Mediterranean high-mountain lakes, *Limnol. Oceanogr.*, *61*, 413–429, doi:10.1002/lno.10204.

Erga, S. R., K. Aursland, Ø. Frette, B. Hamre, J. K. Lotsberg, J. J. Stamnes, J. Aure, F. Rey, and K. Stamnes (2005), UV transmission in Norwegian marine waters: Controlling factors and possible effects on primary production and vertical distribution of phytoplankton, *Mar. Ecol. Prog. Ser.*, *305*, 79–100, doi:10.3354/meps305079.

Figueroa, F. L., J. M. Blanco, F. Jiménez-Gómez, and J. Rodríguez (1997a), Effects of ultraviolet radiation on carbon fixation in Antarctic nanophytoflagellates, *Photochem. Photobiol.*, *66*, 185–189, doi:10.1111/j.1751-1097.1997.tb08641.x.

Figueroa, F. L., J. Mercado, C. Jiménez, S. Salles, J. Aguilera, M. P. Sánchez-Saavedra, M. Lebert, D. Häder, O. Montero, and L. Lubián (1997b), Relationship between bio-optical characteristics and photoinhibition of phytoplankton, *Aquat. Bot.*, *59*, 237–251, doi:10.1016/S0304-3770(97)00065-X.

Finkel, Z. V., J. Beardall, K. J. Flynn, A. Quigg, T. Alwyn, V. Rees, and J. A. Raven (2010), Phytoplankton in a changing world: Cell size and elemental stoichiometry, *J. Plankton Res.*, *32*, 119–137, doi:10.1093/plankt/fbp098.

Gallisai, R., F. Peters, G. Volpe, S. Basart, and J. M. Baldasano (2014), Saharan dust deposition may affect phytoplankton growth in the Mediterranean Sea at ecological time scales, *PLoS One*, *9*(10), e110762, doi:10.1371/journal.pone.0110762.

Gang, L., K. Gao, and G. Gao (2011), Differential impacts of solar UV radiation on photosynthetic carbon fixation from the coastal to offshore surface waters in the South China Sea, *Photochem. Photobiol.*, *87*, 329–334, doi:10.1111/j.1751-1097.2010.00862.x.

Gao, K., G. Li, E. W. Helbling, and V. E. Villafañe (2007), Variability of UVR effects on photosynthesis of summer phytoplankton assemblages from a tropical coastal area of the South China Sea, *Photochem. Photobiol.*, *83*, 802–809, doi:10.1111/j.1751-1097.2007.00154.x.

García-Górriz, E., and M. E. Carr (2001), Physical control of phytoplankton distributions in the Alboran Sea: A numerical and satellite approach, *J. Geophys. Res.*, *106*, 16,795–16,805, doi:10.1029/1999JC000029.

Giorgi, F., and P. Lionello (2008), Climate change projections for the Mediterranean region, *Global Planet. Change*, *63*, 90–104, doi:10.1016/j.gloplacha.2007.09.005.

Giovagnetti, V., C. Brunet, F. Conversano, F. Tramontano, I. Obernosterer, C. Ridame, and C. Guieu (2013), Assessing the role of dust deposition on phytoplankton ecophysiology and succession in a low-nutrient low-chlorophyll ecosystem: A mesocosm experiment in the Mediterranean Sea, *Biogeosciences*, *10*, 2973–2991, doi:10.5194/bg-10-2973-2013.

Grossman, A. R., K. R. M. Mackey, and S. Bailey (2010), A perspective on photosynthesis in the oligotrophic oceans: Hypotheses concerning alternate routes of electron flow, *J. Phycol.*, *46*, 629–634, doi:10.1111/j.1529-8817.2010.00852.x.

Guieu, C., et al. (2010), Large clean mesocosms and simulated dust deposition: A new methodology to investigate responses of marine oligotrophic ecosystems to atmospheric inputs, *Biogeosciences*, *7*, 2765–2784, doi:10.5194/bg-7-2765-2010.

Häder, D. P., E. W. Helbling, C. E. Williamson, and R. C. Worrest (2011), Effects of UV radiation on aquatic ecosystems and interactions with climate change, *Photochem. Photobiol. Sci.*, *10*, 242–260, doi:10.1039/C0PP90036B.

Häder, D. P., V. E. Villafañe, and E. W. Helbling (2014), Productivity of aquatic primary producers under global climate change, *Photochem. Photobiol. Sci.*, *13*, 1370–1392, doi:10.1039/c3pp50418b.

Helbling, E. W., and H. E. Zagarese (2003), *UV Effects in Aquatic Organisms and Ecosystems*, The Royal Society of Chemistry, Cambridge, U. K., doi:10.1039/9781847552266.

Helbling, E. W., B. E Chalkerb, C. Dunlapb, O. Holm-Hansen, and V. E. Villafañe (1996), Photoacclimation of Antarctic marine diatoms to solar ultraviolet radiation, *J. Exp. Mar. Biol. Ecol.*, *204*, 85–101, doi:10.1016/0022-0981(96)02591-9.

Helbling, E. W., P. Carrillo, J. M. Medina-Sánchez, C. Durán, G. Herrera, M. Villar-Argaiz, and V. E. Villafañe (2013), Interactive effects of vertical mixing, nutrients and ultraviolet radiation: In situ photosynthetic responses of phytoplankton from high mountain lakes in southern Europe, *Biogeosciences*, *10*, 1037–1050, doi:10.5194/bg-10-1037-2013.

Hessen, D., H. De Lange, and E. Van Donk (1997), UV-induced changes in phytoplankton cells and its effects on grazers, *Freshwater Biol.*, *38*, 513–524, doi:10.1046/j.1365-2427.1997.00223.x.

Houpert, L., P. Testor, X. Durrieu de Madrona, S. Somot, F. D'Ortenzio, C. Estournel, and H. Lavigne (2015), Seasonal cycle of the mixed layer, the seasonal thermocline and the upper-ocean heat storage rate in the Mediterranean Sea derived from observations, *Prog. Oceanogr.*, *132*, 333–352, doi:10.1016/j.pocean.2014.11.004.

Jeffrey, S. W., and G. F. Humphrey (1975), New spectrophotometric equations for determining chlorophylls a, b, c 1 and c 2 in higher plants, algae and natural phytoplankton, *Biochem. Physiol. Pflanz.*, *167*, 191–194.

Jickells, T. D., and C. M. Moore (2015), The importance of atmospheric deposition for ocean productivity, *Annu. Rev. Ecol. Syst.*, *46*, 481–501, doi:10.1146/annurev-ecolsys-112414-054118.

Jickells, T. D., et al. (2005), Global iron connections between desert dust, ocean biogeochemistry, and climate, *Science*, *308*, 67–71, doi:10.1126/science.1105959.

Karentz, D., J. Cleaver, and D. L. Mitchell (1991), Cell survival characteristics and molecular responses of Antarctic phytoplankton to ultraviolet-B radiation, *J. Phycol.*, *27*, 326–341, doi:10.1111/j.0022-3646.1991.00326.x.

Korbee, N., P. Carrillo, M. T. Mata, S. Rosillo, J. M. Medina-Sánchez, and F. Figueroa (2012), Effects of ultraviolet radiation and nutrients on the structure–function of phytoplankton in a high mountain lake, *Photochem. Photobiol. Sci.*, *11*, 1087–1098, doi:10.1039/c2pp05336e.

Koroleff, F. (1977), Simultaneous persulphate oxidation of phosphorus and nitrogen compounds in water, in *Report on the Baltic Intercalibration Workshop*, edited by K. Grasshoff, pp. 52–53, Compiler, Kiel, Germany.

Krause, G. H., and E. Weis (1991), Chlorophyll fluorescence and photosynthesis: The basics, *Annu. Rev. Plant Physiol. Plant Mol. Biol.*, *42*, 313–349, doi:10.1146/annurev.pp.42.060191.001525.

Lekunberri, I., T. Lefort, E. Romero, E. Vazquez-Dominguez, C. Romera-Castillo, C. Marrasé, F. Peters, M. Weinbauer, and J. M. Gasol (2010), Effects of a dust deposition event on coastal marine microbial abundance and activity, bacterial community structure and ecosystem function, *J. Plankton Res.*, *32*, 381–396, doi:10.1093/plankt/fbp137.

Leu, E., S. Falk-Petersen, and D. Hessen (2007), Ultraviolet radiation negatively affects growth but not food quality of arctic diatoms, *Limnol. Oceanogr.*, *52*, 787–797, doi:10.4319/lo.2007.52.2.0787.

Li, T., D. Pan, Y. Bai, G. Li, X. He, C.-T. A. Chen, K. Gao, D. Liu, and H. Lei (2015), Satellite remote sensing of ultraviolet irradiance onthe ocean surface, *Acta Oceanolog. Sin.*, *34*(6), 101–112, doi:10.1007/s13131-015-0690-z.

Lignell, R. (1992), Problems in filtration fractionation of ^{14}C primary productivity samples, *Limnol. Oceanogr.*, *37*, 172–178, doi:10.4319/lo.1992.37.1.0172.

Llabrés, M., and S. Agustí (2006), Picophytoplankton cell death induced by UV radiation: Evidence for oceanic Atlantic communities, *Limnol. Oceanogr.*, *51*, 21–29, doi:10.4319/lo.2006.51.1.0021.

Mackey, K. R. M., T. Rivlin, A. R. Grossman, A. F. Post, and A. Paytan (2009), Picophytoplankton responses to changing nutrient and light regimes during a bloom, *Mar. Biol.*, *156*, 1531–1546, doi:10.1007/s00227-009-1185-2.

Mackey, K. R. M., C. T. Chien, A. F. Post, M. A. Saito, and A. Paytan (2015), Rapid and gradual modes of aerosol trace metal dissolution in seawater, *Front. Microbiol.*, *5*(794), 1–11, doi:10.3389/fmicb.2014.00794.

Marañón, E., et al. (2010), Degree of oligotrophy controls the response of microbial plankton to Saharan dust, *Limnol. Oceanogr.*, *55*, 2339–2352, doi:10.4319/lo.2010.55.6.2339.

Maxwell, K., and G. N. Johnson (2000), Chlorophyll fluorescence—A practical guide, *J. Exp. Bot.*, *51*, 659–668, doi:10.1093/jexbot/51.345.659.

Mercado, J. M., T. Ramírez, D. Cortés, M. Sebastián, and M. Vargas-Núñez (2005), Seasonal and inter-annual variability of the phytoplankton communities in an upwelling area of the Alborán Sea (SW Mediterranean Sea), *Sci. Mar.*, *69*, 451–465.

Mercado, J. M., T. Ramírez, D. Cortés, M. Sebastián, A. Reul, and B. Bautista (2006), Diurnal changes in the bio-optical properties of the phytoplankton in the Alboran Sea (Mediterranean Sea), *Estuarine Coastal Shelf Sci.*, *69*, 459–470, doi:10.1016/j.ecss.2006.05.019.

Moore, C. M., M. M. Mills, R. Langlois, A. Milne, E. P. Achterberg, J. La Roche, and R. J. Geider (2008), Relative influence of nitrogen and phosphorus availability on phytoplankton physiology and productivity in the oligotrophic sub-tropical North Atlantic Ocean, *Limnol. Oceanogr.*, *53*(1), 291–305, doi:10.4319/lo.2008.53.1.0291.

Morales-Baquero, R., E. Pulido-Villena, and I. Reche (2006), Atmospheric inputs of phosphorus and nitrogen to the southwest Mediterranean region: Biogeochemical responses of high mountain lakes, *Limnol. Oceanogr.*, *51*, 830–837, doi:10.4319/lo.2006.51.2.0830.

Morán, X. A. G., A. López-Urrutia, A. Calvo-Díaz, and W. K. W. Li (2010), Increasing importance of small phytoplankton in a warmer ocean, *Global Change Biol.*, *16*, 1137–1144, doi:10.1111/j.1365-2486.2009.01960.x.

Mukhopadhyay, S., and P. Kreycik (2008), Dust generation and drought patterns in Africa from helium-4 in a modern Cape Verde coral, *Geophys. Res. Lett.*, *35*, L20820, doi:10.1029/2008GL035722.

Packard, T. T., et al. (1988), Formation of the Alboran oxygen minimum zone, *Deep Sea Res., Part A*, *35*, 1111–1118, doi:10.1016/0198-0149(88)90003-9.

Paytan, A., K. R. M. Mackey, Y. Chen, I. D. Lima, S. C. Doney, N. Mahowald, R. Labiosa, and A. F. Post (2009), Toxicity of atmospheric aerosols on marine phytoplankton, *Proc. Natl. Acad. Sci. U.S.A.*, *106*, 4601–4605, doi:10.1073/pnas.0811486106.

Peralta-Ferriz, C., and R. A. Woodgate (2015), Seasonal and interannual variability of pan-Arctic surface mixed layer properties from 1979 to 2012 from hydrographic data, and the dominance of stratification for multiyear mixed layer depth shoaling, *Prog. Oceanogr.*, *134*, 19–53, doi:10.1016/j.pocean.2014.12.005.

Piggott, J. J., C. R. Townsend, and C. D. Matthaei (2015), Reconceptualizing synergism and antagonism among multiple stressors, *Ecol. Evol.*, *5*, 1538–1547, doi:10.1002/ece3.1465.

Prospero, J. M., and P. J. Lamb (2003), African droughts and dust transport to the Caribbean: Climate change implications, *Science*, *302*, 1024–1027, doi:10.1126/science.1089915.

Pulido-Villena, E., I. Reche, and R. Morales-Baquero (2006), Significance of atmospheric inputs of calcium over the southwestern Mediterranean region: High mountain lakes as tools for detection, *Global Biogeochem. Cycles*, *20*, GB2012, doi:10.1029/2005GB002662.

Pulido-Villena, E., T. Wagener, and C. Guieu (2008), Bacterial response to dust pulses in the western Mediterranean: Implications for carbon cycling in the oligotrophic ocean, *Global Biogeochem. Cycles*, *22*, GB1020, doi:10.1029/2007GB003091.

Raven, J. A. (1998), The twelfth Tansley Lecture. Small is beautiful: The picophytoplankton, *Funct. Ecol.*, *12*, 503–513, doi:10.1046/j.1365-2435.1998.00233.x.

Ribera D'Alcalà, M., G. Civitarese, F. Conversano, and R. Lavezza (2003), Nutrient ratios and fluxes hint at overlooked processes in the Mediterranean Sea, *J. Geophys. Res.*, *108*(C9), 8106, doi:10.1029/2002JC001650.

Ribés, M., R. Coma, and J. M. Gili (1999), Seasonal variation of particulate organic carbon, dissolved organic carbon and the contribution of microbial communities to the live particulate organic carbon in a shallow near bottom ecosystem in the Northwestern Mediterranean Sea, *J. Plankton Res.*, *21*, 1077–1100, doi:10.1093/plankt/21.6.1077.

Ridame, C., J. Dekaezemacker, C. Guieu, S. Bonnet, S. L´Helguen, and F. Malien (2014), Contrasted saharan dust events in LNLC environments: Impact on nutrient dynamics and primary production, *Biogeosciences*, *11*, 4783–4800, doi:10.5194/bg-11-4783-2014.

Romero, E., F. Peters, C. Marrasé, O. Guadayol, J. M. Gasol, and M. Weinbauer (2011), Coastal Mediterranean plankton stimulation dynamics through a dust storm event: An experimental simulation, *Estuarine Coastal Shelf Sci.*, *93*, 27–39, doi:10.1016/j.ecss.2011.03.019.

Sarhan, T., J. García Lafuente, M. Vargas, J. M. Vargas, and F. Plaza (2000), Upwelling mechanisms in the northwestern Alboran Sea, *J. Mar. Syst.*, *23*, 317–331, doi:10.1016/S09247963(99)00068-8.

Shao, Y., K. H. Wyrwoll, A. Chappell, J. Huang, Z. Lin, G. H. McTainsh, M. Mikami, T. Y. Tanaka, X. Wang, and S. Yoon (2011), Dust cycle: An emerging core theme in Earth system science, *Aeolian Res.*, *2*, 181–204, doi:10.1016/j.aeolia.2011.02.001.

Sinha, R. P., and D. P. Häder (2008), UV-protectants in cyanobacteria, *Plant Sci.*, *174*, 278–289, doi:10.1016/j.plantsci.2007.12.004.

Sobrino, C., M. Segovia, P. Neale, J. M. Mercado-Carmona, C. García-Gómez, G. Kulk, M. R. Lorenzo, T. Camarena, W. Van de Poll, and K. Spilling (2014), Effect of CO_2, nutrients and light on coastal plankton IV: Physiological responses, *Aquat. Biol.*, *22*, 77–93, doi:10.3354/ab00590.

Stawiarski, B. (2014), Light and temperature induced variability of the elemental composition of picophytoplankton and their minimum requirements based on nutrient limitation experiments, doctoral thesis, The physiological response of picophytoplankton to light, temperature and nutrients, including climate change model simulations.

Steemann Nielsen, E. (1952), The use of radio-active carbon (C^{14}) for measuring organic production in the sea, *J. Cons., Cons. Int. Explor. Mer.*, *18*, 117–140, doi:10.1093/icesjms/18.2.117.

Strzepek, R. F., and P. J. Harrison (2004), Photosynthetic architecture differs in coastal and oceanic diatoms, *Nature*, *43*, 689–692, doi:10.1038/nature02954.

Tanhua, T., D. Hainbucher, K. Schroeder, V. Cardin, M. Alvarez, and G. Civitarese (2013), The Mediterranean Sea system: A review and an introduction to the special issue, *Ocean Sci.*, *9*, 789–803, doi:10.5194/os-9-789-2013.

Tedetti, M., and R. Sempéré (2006), Penetration of ultraviolet radiation in the marine environment. A review, *Photochem. Photobiol.*, *82*, 389–397, doi:10.1562/2005-11-09-IR-733.

Thomas, D. N., M. E. M. Baumann, and M. Gleitz (1992), Efficiency of carbon assimilation and photoacclimation in a small unicellular *Chaetoceros* species from the Weddell Sea (Antarctica): Influence of temperature and irradiance, *J. Exp. Mar. Biol. Ecol.*, *157*, 195–209, doi:10.1016/0022-0981(92)90162-4.

Vaulot, D., C. Courties, and F. Partensky (1989), A simple method to preserve oceanic phytoplankton for flow cytometric analyses, *Cytom. (N.Y.)*, *10*, 629–635, doi:10.1002/cyto.990100519.

Winder, M. (2009), Photosynthetic picoplankton dynamics in Lake Tahoe: Temporal and spatial niche partitioning among prokaryotic and eukaryotic cells, *J. Plankton Res.*, *31*, 1307–1320, doi:10.1093/plankt/fbp074.

Wu, Y., Z. Li, W. Du, and K. Gao (2016), Physiological response of marine centric diatoms to ultraviolet radiation, with special reference to cell size, *J. Photochem. Photobiol. B*, *153*, 1–6, doi:10.1016/j.jphotobiol.2015.08.035.